One-step synthesis of graphene via catalyst-free gas-phase hydrocarbon detonation

2013 Nanotechnology 24 245602

(http://iopscience.iop.org/0957-4484/24/24/245602)

Nanotechnology **24** (2013) 245602 (7pp) doi:10.1088/0957-4484/24/24/245602

One-step synthesis of graphene via catalyst-free gas-phase hydrocarbon detonation

Arjun Nepal[1], Gajendra P Singh[1,2], Bret N Flanders[1] and C M Sorensen[1]

[1] Department of Physics, Kansas State University, Manhattan, KS 66506, USA
[2] Centre for Nanotechnology, Central University of Jharkhand, Ranchi-835205, Jharkhand, India

E-mail: sor@phys.ksu.edu

Received 26 September 2012, in final form 24 March 2013
Published 20 May 2013
Online at stacks.iop.org/Nano/24/245602

Abstract
A one-step, gas-phase, catalyst-free detonation of hydrocarbon (C_2H_2) method was developed to produce gram quantities of pristine graphene nanosheets (GNs). The detonation of C_2H_2 was carried out in the presence of O_2. The molar ratios of O_2/C_2H_2 were 0.4, 0.5, 0.6, 0.7 and 0.8. The obtained GNs were analyzed by XRD, TEM, XPS and Raman spectroscopy. The GNs are crystalline with a (002) peak centered at 26.05° ($d = 0.341$ nm). TEM shows that the GNs are stacked in two to three layers and sometimes single layers. An increase in the size of the GNs (35–250 nm) along with a reduction in defects (Raman $I_D/I_G \sim 1.33$–0.28) and specific surface area (187–23 $m^2\ g^{-1}$) was found with increasing O_2 content. The high temperature of the detonation, ca. 4000 K, is proposed as the cause of graphene production rather than normal soot. The method allows for the control of the number of layers, shape and size of the graphene nanosheets. The process can be scaled up for industrial production.

S Online supplementary data available from stacks.iop.org/Nano/24/245602/mmedia

(Some figures may appear in colour only in the online journal)

1. Introduction

Graphene is a two-dimensional monolayer of sp^2 bonded carbon atoms in a hexagonal crystal structure. It has been drawing considerable interest because of its unique physical properties including excellent mechanical strength, high intrinsic carrier mobility at room temperature, and electrical and thermal conductivity comparable to the in-plane value of graphite [1–3]. These properties open gateways for the potential applications of graphene in technological areas such as nanoelectronics [4, 5], sensors [6], nanocomposites [7, 8], batteries [9], supercapacitors, and hydrogen storage [10]. Pioneering work for the production of graphene was first done by the micromechanical cleavage of highly ordered pyrolytic graphite (HOPG) [10, 11]. However, the low yield makes it unsustainable for large scale use. Numerous methods for preparation of graphene nanosheets have since been developed including chemical vapor deposition (CVD) [12, 13], ultrasonication-assisted exfoliation of graphene oxide (GO) from graphite oxide in water [14], epitaxial growth on an electrically insulating surface [15], solution-based chemical reduction of GO [16], rapid thermal exfoliation of expanded graphite into graphene [17], high temperature heating of polymer on metal/insulator surface [18], and gas-phase plasma synthesis [19]. Notably, the CVD method has been used in a roll-to-roll production of 30 inch monolayer graphene films [20].

For the production of large quantities of graphene, the modified Hummer's method for the production of GO through chemical exfoliation of graphite to graphite oxide and then graphite oxide to GO has gained much attention due to low-cost and higher yield in comparison to other methods [21–24]. However, this method is not ideal because the GO produced suffers from some important drawbacks such as poor electrical conductivity due to the presence of epoxide, carboxyl, and hydroxyl groups on the graphene sheets [2]. Further, the reduction of GO to graphene needs insalubrious chemical reductants such as hydrazine

or sodium borohydride, and high temperature heating in order to recover the graphitic structure [25]. Moreover, the reduction process cannot completely remove the many structural defects introduced by the oxidation process. A few environmentally friendly processes are available to reduce GO to graphene either by chemical or electrochemical methods, but these give low yield [26]. Thus despite the usefulness of previous graphene synthetic methods, none appear economical, eco-friendly, kilogram scale production of the material.

Here we report a novel, cost-effective and eco-friendly, one-step method that involves controlled gas-phase hydrocarbon (C_2H_2) detonation with oxygen (O_2) for the production of graphene nanosheets. Our process has several advantages such as simplicity, high productivity, economic viability, and short synthesis time (minute). This method is catalyst-free and does not generate any toxic by-products during synthesis as generated in solution phase methods [20–24].

2. Experimental details

Graphene nanosheets (GNs) in the form of a powder were prepared from the catalyst-free controlled detonation of C_2H_2 gas in the presence of O_2 in a 16.6 l cylindrical aluminum chamber. The pre-detonation molar ratios of O_2/C_2H_2 were 0.4, 0.5, 0.6, 0.7, and 0.8. For each ratio, the initial chamber pressure was 1 atmosphere. The gases had purities of 98.0% for C_2H_2 and 99.0% for O_2. In a typical batch, the detonation of C_2H_2 with O_2 was carried out by a controlled power supply through a spark generator ignition system (figures S1 and S2, where S refers supplementary information available at stacks.iop.org/Nano/24/245602/mmedia). During the detonation, the hydrocarbon was first converted into free carbon atoms or ions which condensed into a nanoparticle carbon aerosols which in turn quickly aggregated and then finally formed a gel, known as a carbon aerosol gel (CAG) [27]. After the detonation, the chamber was allowed to cool to 300 K. The fluffy black CAG powder was collected from the chamber (inset figure 5); we will henceforth call this material 'detonation carbon'. The material was homogeneous and subsequent characterization confirmed that it was one phase. The detonation pressure and temperature were measured with a data acquisition system. The same process was followed for all molar ratios. Table 1 shows the peak temperature and the pressure observed during detonation for different O_2/C_2H_2 molar ratios. These high pressures and temperatures (ca. 4000 K), which are a consequence of the exothermic detonation of the hydrocarbon and oxygen, last for about 15 ms during the detonation, after which the system rapidly cools (figure S2 available at stacks.iop.org/Nano/24/245602/mmedia). The phase, layered structure, and the chemical compositions of detonation carbon was analyzed by XRD, TEM, Raman spectroscopy and x-ray photoelectron spectroscopy.

3. Characterizations

X-ray diffraction was carried out using a Bruker D8 advance x-ray diffractometer, Germany, with nickel filter Cu Kα radiation as the x-ray source to determine phase purity and degree of crystallization. The morphology and the size of the samples were determined with a FEI Company Nova NanoSEM 430 field emission scanning electron microscope, FESEM, at 3.5 kV and low vacuum with a TLD detector and Philips CM-100 transmission electron microscope (TEM) with an accelerating voltage of 100 kV. For TEM measurement, the samples were prepared by inserting Cu grids in the detonation carbon powder without using any solvent. The high resolution TEM images and SAED patterns were recorded by using FEI Tecnai F20 XT field emission transmission electron microscope with an accelerating voltage of 200 kV. BET measurements were carried out using a Nova 1000 series surface area analyzer, Quantachrome instrument. Diffuse reflectance FTIR spectra were recorded via a Cary 630 FTIR spectrophotometer, Agilent Technology, USA over a range 500–4000 cm^{-1}. The x-ray photoelectron spectroscopy (XPS) of a Perkin-Elmer PHI 5400 spectrometer with Al Kα x-ray source (1486.6 eV) was used to obtain the chemical compositions of the samples. The spectrometer was calibrated using Au $4f_{7/2}$ at 84.0 eV and Cu $2p_{3/2}$ at 932.7 eV. The base pressure of the analysis chamber was below 10^{-9} mbar. The room temperature Raman spectra were obtained on pellets of 10 mm diameter and 2 mm thick (as shown in the inset of figure 8) with an iHR550 Raman spectrophotometer, Horiba Jobin Yvon with a HeNe laser (632.8 nm) as the excitation source.

Table 1. The molar ratio O_2/C_2H_2, peak detonation temperature (T_d) and pressure (P_d) for preparation of GNs.

Molar ratio O_2/C_2H_2	T_d (K) (±200 K)	P_d (atm) (±1.5 atm)
0.4	3800	13.4
0.5	3900	13.1
0.6	4200	13.8
0.7	3600	14.3
0.8	3800	14.3

4. Results and discussion

The x-ray diffraction (XRD) patterns of the detonation carbon obtained at O_2/C_2H_2 of 0.4, 0.5, 0.6, 0.7, and 0.8 and graphite flakes (GF, obtained from Alfa Aesar for comparison) are depicted in figure 1. Figure 1(a) shows seven well defined diffraction peaks that are characteristic of graphite with the most intense (002) peak centered at 26.6° (enlarged in the inset), while the (002) peak of the detonation carbon is centered at 26.05° (figures 1(b)–(f)) to imply an interplanar spacing (d) of 0.341 nm, which is larger than $d = 0.335$ nm of GF. The determined $d = 0.341$ nm for the detonation carbon is in good agreement with the XRD pattern reported for pristine GNs synthesized by other methods [28, 29]. Hence, the detonation carbon resembles the graphitic (graphene) structure. In addition, the reduction in full width at half maxima (FWHM) of the (002) peak with increasing O_2/C_2H_2 ratio indicates an increased size of the crystallite and, thus, more crystalline order.

Figures 2(a)–(e) shows TEM images of the detonation carbon powder obtained at different O_2/C_2H_2 gas ratios.

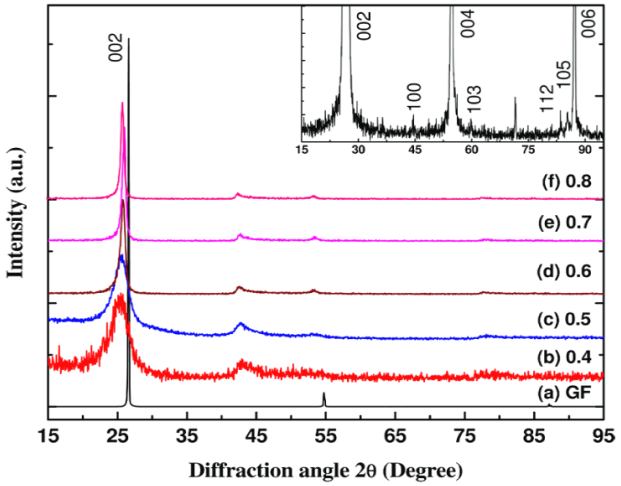

Figure 1. XRD patterns of (a) graphite flakes (GF), and ((b)–(f)) the detonation carbon graphene nanosheets (GNs) prepared by detonation with different O_2/C_2H_2 molar ratios. The magnified spectrum of (a) is shown in the inset.

All images reveal that the layers in detonation carbon are transparent, crumpled, folded, and randomly stacked on each other. They show a laminar morphology with crumpling consistent with the structure of pristine two-dimensional graphene prepared by other methods [28–30]. This crumpling is intrinsic to graphene sheets because a thermodynamically unstable two-dimensional sheet undergoes microscopic crumpling via bending or buckling to get thermodynamically stable three-dimensional structures in localized regions [31]. In figures 2(a) and (b), the detonation carbon prepared with O_2/C_2H_2 = 0.4 and 0.5, respectively, show transparent ramified fractal aggregates of GNs. These aggregates have dense regions about 35–55 nm size connected by thin, continuous, twisted, ribbon-like structures (see figures S3(a) and (b) available at stacks.iop.org/Nano/24/245602/mmedia). This implies that the detonation carbon consists of GNs interlaced with one another. With increasing ratios from 0.6 to 0.8, the GNs show a distinct feature of nearly circular shape with an increased size of about 225–250 nm (figures 2(c)–(e) and S3(c)–(e) available at stacks.iop.org/Nano/24/245602/mmedia). The similar layer morphology stacked over each other around 250–350 nm size of the GNs powder prepared from O_2/C_2H_2 of 0.8 is observed in FESEM as shown in figure S4 (available at stacks.iop.org/Nano/24/245602/mmedia). The O_2/C_2H_2 ratio dependence of GNs size observed in TEM images is consistent with the (002) peak widths in the XRD spectra (figures 1(b)–(f)). Thus, the detonation carbon appears to be composed of GNs and will hereafter be referred to as such as well. Moreover, in the samples of lower O_2/C_2H_2, the randomly oriented GNs (figures 2(a) and (b)) exhibit many thin layers entangled with each other with overlapped edges, while more ordered stacking of GNs in mostly two to three layers is observed for the samples of higher O_2/C_2H_2 as seen in figures 2(c)–(e). The HRTEM image of the edge of the GNs in figure 2(f) shows the layer structure more closely.

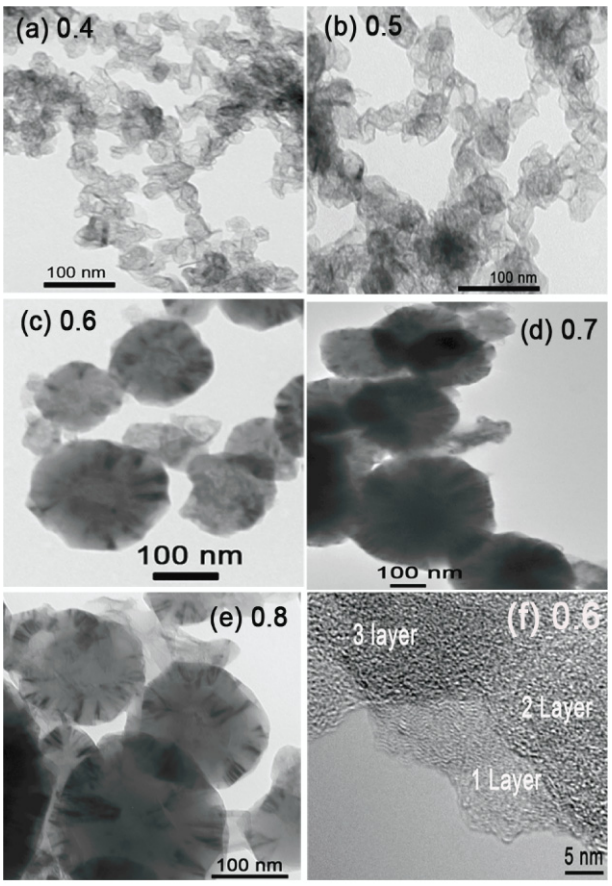

Figure 2. TEM images of GNs prepared by detonation of different molar ratios of O_2/C_2H_2 (a)–(e). (f) HRTEM image of GNs at 0.6 shows well the number of layers.

High magnification TEM images and the SAED patterns of the GNs of selected regions are shown in figure 3. The transparent and featureless regions, indicated by arrows in figures 3(a) and (d), are likely to be monolayer graphene which tends to scroll at the edges. The SAED patterns in figures 3(b), (c) and (f) confirm the crystalline structure of the GNs. The diffraction patterns of the region marked with 'A' and 'C' in figure 3(a) and (e) show six-fold symmetry (see figures 3(b) and (f)) similar to monolayer graphene, whereas the region marked with 'B' in figure 3(a) shows misaligned diffraction spots in tiny arc shapes representing randomized six-fold symmetry as shown in figure 3(c). The misaligned spots could probably be due to crumpled local regions in GNs. The HRTEM images of GNs depicted in figure S3(f) (available at stacks.iop.org/Nano/24/245602/mmedia) shows the lattice fringes spacing of 0.240 nm which is in good agreement with the in-plane lattice constant of 0.246 nm for graphite [32].

The Brunauer–Emmett–Teller (BET) specific surface area (SSA) of the GNs measured from N_2 adsorption desorption isotherms at 77 K is shown in figure 4. The isotherms exhibit type-II pattern and type H3 hysteresis loop. The adsorption hysteresis suggests that the isotherm is a pseudotype-II pattern due to multi-layer adsorption in materials having slit-like pores or aggregates of platy

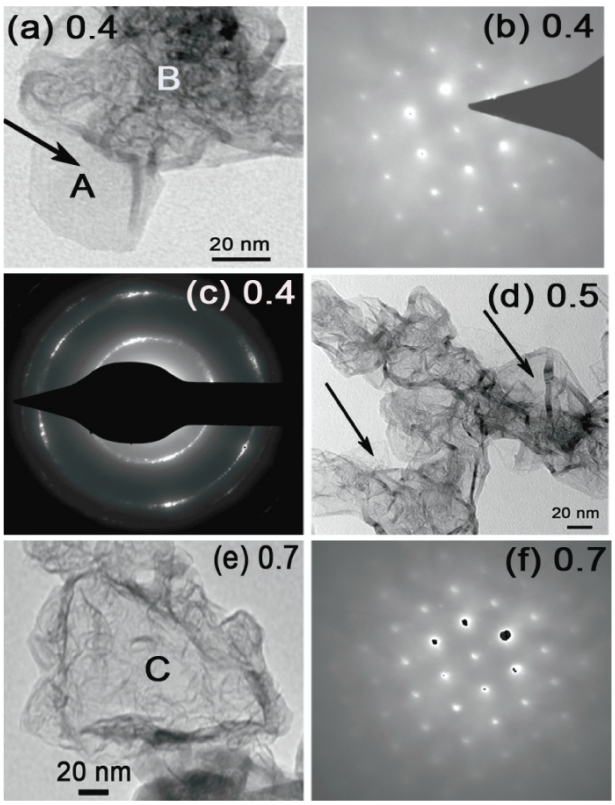

Figure 3. High magnification TEM images and SAED patterns of GNs prepared by detonation of different molar ratios of O_2/C_2H_2 (a)–(f). The SAED patterns of regions marked with 'A', 'B', and 'C' are shown in (b), (c) and (f), respectively. Arrows indicate the monolayer GNs.

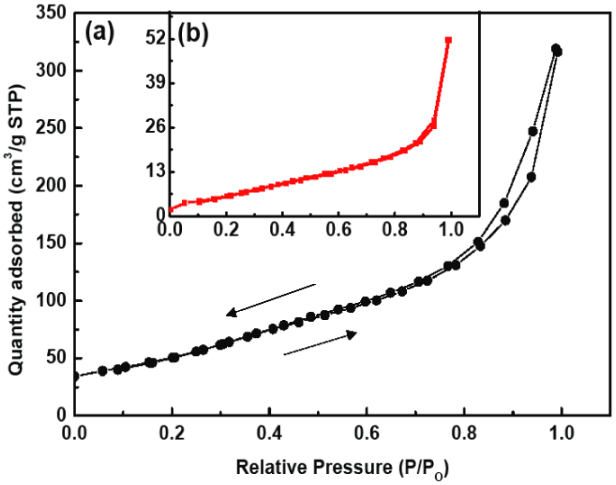

Figure 4. Nitrogen adsorption desorption isotherm of GNs prepared by detonation of O_2/C_2H_2 of (a) 0.4 and (b) 0.8.

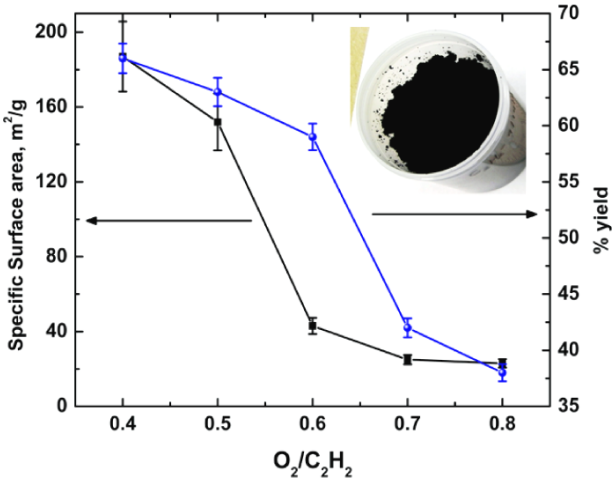

Figure 5. The specific surface area and yield of GNs powder. Lines are guides to the eye. Inset shows the bulk quantity ~7.4 g graphene powder collected after a detonation.

particles [33]. In graphene, adsorption occurs on the surface of the graphene sheets, but due to their few layered structure, slit-like open pores exist. These open pores are responsible for the hysteresis loop observed in graphene materials [34]. From the linear region of the graph and using the BET equation, it is found that the SSA lies in between 23 and 187 $m^2\ g^{-1}$ (figure 5), which is significantly lower than the theoretical SSA of 2630 $m^2\ g^{-1}$ for individual isolated graphene sheets [35]. However, the SSA of the detonation carbon prepared at 0.4 O_2/C_2H_2 is close to the previously reported SSA-value of 184 $m^2\ g^{-1}$ for GNs [36]. A significant finding is that the yield per detonation of the GNs is high, in the range of 38%–66% as shown in figure 5. It is found that the mass of the GNs is decreased as the amount of O_2 is increased in the gaseous mixture.

The Drifts-FTIR measurement was performed to explore the surface functional groups present on GNs produced by detonation. Figure 6 displays the Drifts-FTIR spectra of detonation carbon prepared with different O_2/C_2H_2 ratio. As the production method involves C_2H_2 and O_2, one might expect some carboxyl or epoxy groups and hydrogen attached to the surface of GNs. However, the spectra (figure 6) do not show any features of functional group attached to the surface of the detonation carbon GNs, suggesting its pristine nature. The chemical composition of GNs is further explored by x-ray photoelectron spectroscopy (XPS). The XPS spectra of graphene GNs obtained after detonation of O_2/C_2H_2 of 0.4 is presented in figure 7. The survey XPS spectrum in figure 7(a) indicates that the graphene is very pure because the actual ratio of C to O is about 49:1. Since XPS measures the composition on the sample surface, the presence of trace oxygen in the survey spectrum can be influenced by the moisture absorption on the surface from the atmosphere [37–39]. However, the enlarged view of the C 1s spectrum presented in figure 7(b) shows a single peak around 284.8 eV, which is associated with graphitic carbon. Moreover, the asymmetry in the peak is due to structural disorder at the edges of the sp^2 network in graphene where the plane of carbon and any carbon fragments could be interacting with the surface oxygen attached during the transfer of the sample to the XPS instrument. No additional signals are observed (see figure S5 available at stacks.iop.org/Nano/24/245602/mmedia for XPS of O_2/C_2H_2 of 0.8 as well) to imply that no other functional groups are attached with

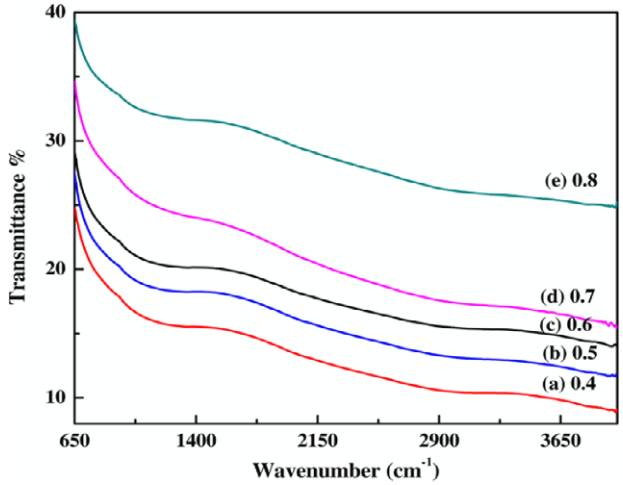

Figure 6. Drifts-FTIR spectra of GNs prepared by detonation of different molar ratios of O_2/C_2H_2.

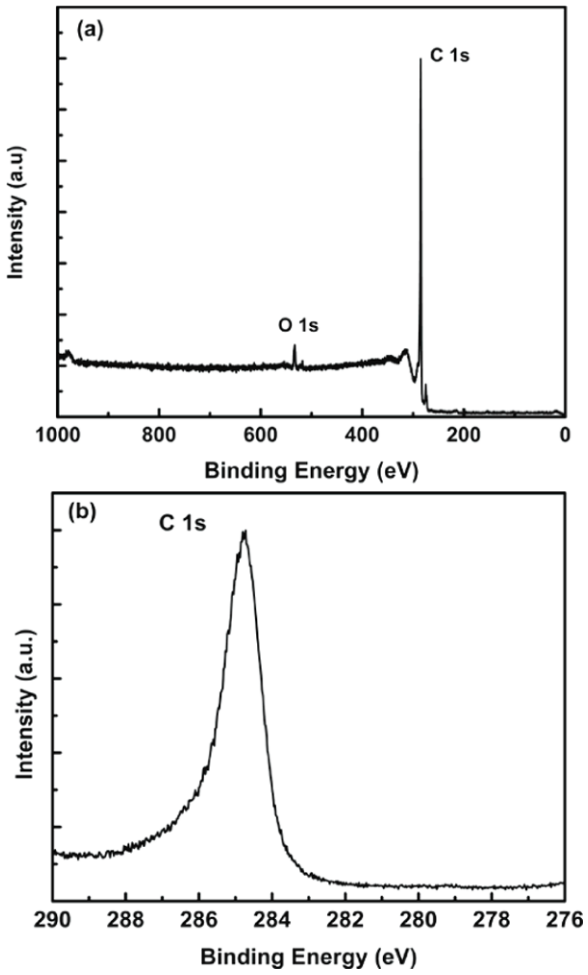

Figure 7. XPS spectra of graphene powder prepared after detonation of O_2/C_2H_2 of 0.4, (a) survey and (b) C 1s spectrum detail.

the C–C system of GNs. This is consistent with the FTIR data mentioned above. These results confirm the one phase, pristine nature of the GNs produced here.

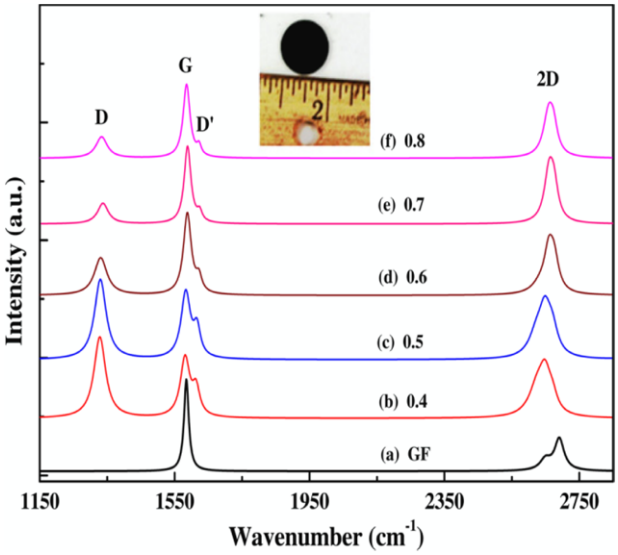

Figure 8. Raman spectra of GF and pristine GNs prepared by detonation of different molar ratios of O_2/C_2H_2. The inset shows the pellet form of GNs powder for Raman measurement.

The structure and quality of the detonation carbon GNs were analyzed by using Raman spectroscopy. Figure 8 shows the Raman spectra of GF and the detonation carbon GNs measured at an excitation wavelength of 632.8 nm under ambient conditions. Figure 8(a) presents characteristic G- and 2D-bands of GF at 1584 and 2690 cm^{-1}, respectively, and the absence of defect (D) band indicates that GF are almost defect free. The sharp G-band at 1584 cm^{-1} corresponds to an optical E_{2g} phonon at the Brillouin zone center of all sp^2 hybridized carbons, while the 2D-band at 2690 cm^{-1} corresponds to overtones of the D-band. This band is present even in absence of defects because it is the sum of two phonons with opposite momentum [40, 41]. It is the most prominent feature for graphene in the Raman spectrum, and its position and shape can be used to distinguish between single-layer, double-layer and few-layer graphene with AB interlayer stacking [30, 40].

As shown in figures 8(b)–(f), the Raman spectra of the detonation carbon GNs show two new bands at 1328 and 1610 cm^{-1} along with G- and 2D-bands at 1580 and 2650 cm^{-1}. The band at 1328 cm^{-1} is assigned to the D-band, which is due to an intervalley double resonance (DR) Raman process from the transverse optical modes of K-point phonons of A_{1g} symmetry in a structural defect or partially disordered structures of the sp^2 domains in GNs [40, 41]. The peak at 1610 cm^{-1} is called the D′-band that occurs via an intravalley DR process in the presence of defects. Furthermore, the relative intensity of D- and G-bands is a convenient way to estimate the extent of defects and the size of in-plane sp^2 domain in the GNs [31, 42]. An obvious observation is that the intensity of the D-band decreases with increasing O_2 content. The intensity ratio of the D- and G-bands (I_D/I_G) in GNs decreases from 1.33 to 0.28 for 0.4 to 0.8 O_2/C_2H_2 ratio. This indicates that partial sp^2 domains are restored at different levels, and the graphitic degree of GNs is also improved accordingly due to the

reduction effect and self-repairing of the graphene layer at high O_2 content [29]. The shape of the 2D-band is O_2 content dependent. At 0.4 O_2/C_2H_2, the 2D-band is broad to imply many layers of GNs, as is also evident from TEM images in figure S3(a) (available at stacks.iop.org/Nano/24/245602/mmedia). The width gradually decreases from 65 to 43 cm^{-1} (see figure S6 available at stacks.iop.org/Nano/24/245602/mmedia) with increasing O_2 content, becoming sharpest for 0.8 O_2/C_2H_2. This evolution of sharpness of the 2D-band implies the transformation of GNs from many layers to two to three layers with increasing O_2 content (the width of the 2D-band for monolayer graphene is 24 cm^{-1}) [43]. Hence, it can be concluded that O_2 plays a vital role for GNs quality in this particular process.

The question remains why graphene is created in this detonation process instead of normal carbonaceous soot. The mechanism of graphene production is undoubtedly as difficult to describe as the mechanism of soot formation in flames, a description which remains incomplete [44]. However, an important clue to a description might lie in table 1 which shows the peak temperatures and pressures observed during detonation for the different molar ratios of O_2/C_2H_2 used. No functionality with molar ratio is observed beyond the estimated errors of the measurements. These temperatures and pressures are consistent with each other under the assumption of no change in the total moles of gas in the chamber from before detonation, at ca. 300 K and 1 atm, to the peak temperature. The peak detonation temperature of about 4000 K is roughly twice the combustion temperature of sooting hydrocarbon/air diffusion flames including C_2H_2 [45]. The 'normal' soot produced in such flames consists of roughly spherical monomers (primary particles) with diameters in the range of 20–50 nm joined together into fractal aggregates [46, 47]. The composition of these monomers is typically mostly carbon with a carbon/hydrogen ratio of $C/H \approx 8$, and the carbon is nearly amorphous being composed of many small graphitic planes [45]. In strong contrast detonation carbon is pure carbon with graphene morphology and characteristics; it is graphene. Based on our temperature measurements we propose that the key difference is the temperature. This hypothesis is supported by the observations of Choi *et al* [48]. They used a burner arrangement in which C_2H_2 co-flowed with an annular oxyhydrogen flame. This flame produced normal soot. The flame was irradiated with a many watt CO_2 laser. Sharply above a laser power threshold the flame stopped producing normal soot and instead produced 'shell-shape carbon nanoparticles' composed of graphenic-like curved layers wrapped together. Concomitant with this threshold, the flame temperature jumped from 2100 to 3000 K. Although these observations are unexplained, their similarity to our detonation process in temperature and resulting morphologies supports our hypothesis that the high temperatures (>3000 K) during detonation is the fundamental cause of the graphenic nature of the carbon produced. Given these observations, we further hypothesize that high temperature, such as 4000 K, completely decomposes the hydrocarbon precursor to yield carbon atoms or ions which then rapidly combine after the high temperature phase to form graphene. This is very different than the current view of normal soot formation in a flame which describes soot formation as a chemical process involving molecular polymerization up a chain of polyaromatic hydrocarbons followed by dehydrogenation to soot [44]. Finally, if this hypothesis is true, detonation of other hydrocarbons should yield graphene materials as well; a proposition we will soon pursue.

5. Conclusions

In summary, a simple, quick, one-step, eco-friendly, high-yield method for the gram scale production of graphene nanosheets has been developed. The method involves the controlled detonation of C_2H_2 in presence of O_2. The high temperature of the detonation, ca. 4000 K, is proposed as the cause of graphene production rather than normal soot. This method is green and does not result in contamination of the graphene product. Simple modification of our lab-scale apparatus could produce 300 g h^{-1}. Thus, with scale up, this method can produce graphene nanosheets in the large quantities required for industrial application.

Acknowledgments

We thank Professor K J Klabunde for use of his XRD and BET instruments and also thank Dr Daniel L Boyle for TEM and FESEM and Dr David Moore, KU for HRTEM measurement, Professor Keith L Hohn and Myles Ikenberry for XPS and Dr Leila Maurmann for FTIR. We also thank to DST, New Delhi, Govt of India, for providing opportunity to Dr G P Singh to visit KSU under BOYSCAST fellowship. This research was partially funded by KSU targeted excellence.

References

[1] Katsnelson M I 2007 *Mater. Today* **10** 20
[2] Ruoff R 2008 *Nature Nanotechnol.* **3** 10
[3] Geim A K 2009 *Science* **324** 1530
[4] Lin Y M, Jenkins K A, Garcia A V, Small J P, Farmer D B and Avouris P 2009 *Nano Lett.* **9** 422
[5] Schedin F, Geim A K, Morozov S V, Hill E W, Blake P, Katsnelson M I and Novoselov K S 2007 *Nature Mater.* **6** 652
[6] Mohanty N and Berry V 2008 *Nano Lett.* **8** 4469
[7] Stankovich S, Dikin D A, Dommett G H B, Kohlhaas K M, Zimney E J, Stach E A, Pinen R D, Nguyen S T and Ruoff R S 2006 *Nature* **442** 282
[8] Watcharotone S, Dikin D A, Stankovich S, Piner R, Jung I, Mommett G H B, Evmenenko G, Wu S E, Chen S F and Liu C P 2007 *Nano Lett.* **7** 1888
[9] Takamura T, Endo K, Fu L, Wu Y P, Lee K J and Matsumoto T 2007 *Electrochim. Acta* **53** 1055
[10] Geim A K and Novoselov K S 2007 *Nature Mater.* **6** 183
[11] Novoselov K S, Jiang D, Schedin F, Booth T J, Khotkevich V V, Morozov S V and Geim A K 2005 *Proc. Natl Acad. Sci. USA* **102** 10451
[12] Charrier A, Coati A, Argunova T, Garreau Y, Pinchaux R, Forbeaux I, Debever J M, Sauvage-Simkin M and Themlin J M 2002 *J. Appl. Phys.* **92** 2479

[13] Berger C, Song Z M, Li X B, Wu X S, Brown N, Naud C, Mayou D, Li T B, Hass J and Marchenko A N 2006 *Science* **312** 1191
[14] Hernandez Y *et al* 2008 *Nature Nanotechnol.* **3** 563
[15] Rutter G M, Crain J N, Guisinger N P, Li T, First P N and Stroscio J A 2007 *Science* **317** 219
[16] Zhu C, Guo S, Fang Y and Dong S 2010 *ACS Nano* **4** 2429
[17] Chen G H, Wenig W G, Wu D and Wu C L 2003 *Eur. Polym. J.* **39** 2329
[18] Chen G H, Wenig W G, Wu D and Wu C L 2003 *Polymer* **44** 1781
[19] Dato A, Radmilovic V, Lee Z, Phillips J and Frenchlach M 2008 *Nano Lett.* **8** 2012
[20] Bae S *et al* 2010 *Nature Nanotechnol.* **5** 574
[21] Park S and Ruoff R S 2009 *Nature Nanotechnol.* **4** 217
[22] Park S, An J, Jung I, Piner R D, An S J, Li X, Velamakanni A and Ruoff R S 2009 *Nano Lett.* **9** 1593
[23] Gomez-Navarro C, Weitz R T, Bittner A M, Scolari M, Mews A, Burghard M and Kern K 2009 *Nano Lett.* **9** 2206
[24] Green A A and Hersam M C 2009 *Nano Lett.* **9** 4031
[25] Stankovich S, Dikin D A, Piner R D, Kohlhaas K A, Kleinhammes A, Jia Y Y, Wu Y, Nguyen S T and Ruoff R S 2007 *Carbon* **45** 1558
[26] Guo H L, Wang X F, Qian Q Y, Wang F B and Xia X H 2009 *ACS Nano* **3** 2653
[27] Dhaubhadel R, Gerving G S, Chakrabarti A and Sorensen C M 2007 *Aerosol Sci. Technol.* **41** 804–10
[28] Wang G, Yang J, Park J, Gou X, Wang B, Liu H and Yao J 2008 *J. Phys. Chem.* C **112** 8192
[29] Sheng Z H, Chen J J, Bo W J, Wang F B and Xia X H 2011 *ACS Nano* **5** 4350
[30] Kaniyoor A and Ramaprabhu S 2011 *J. Appl. Phys.* **109** 124308
[31] Meyer J C, Geim A K, Katsnelson M I, Novoselov K S, Booth T J and Roth S 2007 *Nature* **446** 60
[32] Baskin Y and Meyer L 1995 *Phys. Rev.* **100** 544
[33] Sing K S W 1995 *J. Porous Mater.* **2** 5
[34] Lv W, Tang D-M, He Y-B, You C-H, Shi Z-Q, Chen X-C, Chen C-M, Hou P-X, Liu C and Yang Q-H 2009 *ACS Nano* **3** 3730
[35] Stoller M D, Park S J, Zhu Y W, An J H and Ruoff R S 2008 *Nano Lett.* **8** 3498
[36] Pan D, Wang S, Zhao B, Wu M, Zhang H, Wang Y and Jiao Z 2009 *Chem. Mater.* **21** 3136
[37] Choucair M, Thordarson P and Stride J A 2009 *Nature Nanotechnol.* **4** 30
[38] Tsang S C, Caps V, Paraskevas I, Chadwick D and Thompsett D 2004 *Angew. Chem. Int. Edn* **43** 5645–9
[39] Schniepp H C, Li J-L, McAllister M J, Sai H, Herrera-Alonso M, Adamson D H, Prud'homme R, Car R, Saville D A and Aksay I A 2006 *J. Phys. Chem.* B **110** 8535
[40] Ferrari A C *et al* 2006 *Phys. Rev. Lett.* **97** 187401
[41] Elias D C *et al* 2009 *Science* **323** 610
[42] Luo Z, Yu T, Kim K J, Ni Z, You Y, Lim S, Shen Z, Wang S and Lin J 2009 *ACS Nano* **3** 1781
[43] Malard L M, Pimenta M A, Dresselhause G and Dresselhaus M S 2009 *Phys. Rep.* **473** 51
[44] Frenklach M 2002 *Phys. Chem. Chem. Phys.* **4** 2028
[45] Gaydon A G and Wolfhard H G 1979 *Flames: Their Structure, Radiation and Temperature* 4th edn (London: Chapman and Hall)
[46] Sorensen C M and Feke G D 1996 *Aerosol Sci. Technol.* **25** 328
[47] Dhaubhadel R, Pierce F, Chakrabarti A and Sorensen C M 2006 *Phys. Rev.* E **73** 011404
[48] Choi M, Altman I S, Kim Y J, Pikhitsa P V, Lee S, Park G S, Jeong T and Yoo J B 2004 *Adv. Mater.* **16** 1721